BRDF Analysis of Savanna Vegetation and Salt-Pan Samples

Georgi T. Georgiev, *Member, IEEE*, Charles K. Gatebe, James J. Butler, and Michael D. King, *Senior Member, IEEE*

***Abstract*—In this paper, laboratory-based bidirectional reflectance distribution function (BRDF) analysis of vegetation leaves, soil, and leaf-litter samples is presented. The leaf litter and soil samples, numbered 1 and 2, were obtained from a site located in the savanna biome of South Africa (Skukuza: 25.0° S, 31.5° E). A third soil sample, number 3, was obtained from Etosha Pan, Namibia (19.20° S, 15.93° E, altitude of 1100 m). In addition, BRDF of local fresh and dry leaves from tulip polar tree (*Liriodendron tulipifera*) and black locust tree (*Robinia pseudoacacia*) were studied. It is shown how the BRDF depends on the incident and scatter angles, sample size (i.e., crushed versus whole leaf), soil samples fraction size, sample status (i.e., fresh versus dry leaves), vegetation species (i.e., poplar versus locust), and the vegetation's biochemical composition. As a demonstration of the application of the results of this paper, airborne BRDF measurements acquired with NASA's Cloud Absorption Radiometer over the same general site where the soil and leaf-litter samples were obtained are compared to the laboratory results. Good agreement between laboratory and airborne-measured BRDF is reported.**

***Index Terms*—Bidirectional reflectance distribution function (BRDF), metrology, optical instrumentation and measurements, remote sensing, vegetation.**

I. Introduction

THE MONITORING of land surface is a major science objective in Earth remote sensing. A major goal in land remote sensing is to identify major biomes and to map and distinguish the changes in their composition introduced by anthropogenic and climatic factors. Currently, deforestation and desertification are the most important land-cover-area processes of scientific interest. These processes play a major role in climate variation particularly with respect to clouds and rainfall. Understanding the optical characterization of the biomes properties and their impact on climate variation and, hence, lead to formulation of better site-specific management plans.

The bidirectional reflectance distribution function (BRDF) describes the reflectance of optical materials as a function of incident and scatter angles and wavelength. It is used in modern optical engineering to characterize the spectral and geometrical optical scatter of both diffuse and specular samples. The BRDF is particularly important in the characterization of reflective and transmissive diffusers used in the preflight and on-orbit radiance and reflectance calibration of Earth remote sensing instruments [1]. Satellite BRDF measurements of Earth scenes can be used as a sensitive tool for early detection of changes occurring in vegetation canopies, soils, or the oceans [2]. For example, water-content changes in soil and vegetation can be detected and monitored using BRDF.

In this paper, we analyzed laboratory-based BRDF data of vegetation leaves, leaf litter, and soil samples to study, on a small scale, the effects of view angle distribution and spectral variability in the reflectance of natural biome samples. The samples measured in the laboratory included leaf litter, predominantly from acacia trees, and two different composition regolith soils collected from the savanna biome of Skukuza, South Africa [Fig. 1(a)]. A third soil sample was collected from Etosha Pan, Namibia [Fig. 1(b)]. In addition, BRDF of fresh and dry leaves from the tulip poplar tree (*Liriodendron tulipifera*), poplar hereinafter, and black locust tree (*Robinia pseudoacacia*) located in Maryland, U.S., were studied. The laboratory-based BRDF of all samples was analyzed in the principal plane at 340, 470, and 870 nm, at incident angles of 0° and 67°, and at viewing angles from 0° to 80° for all samples, except the sample from Etosha Pan. The latter has been measured at 412, 555, 667, and 869 nm and at incident angles of 0°, 30°, and 60°. BRDF dependence on the sample particle size was investigated by measuring the following three different samples: whole leaves, samples with leaf particle sizes between 4 and 4.75 mm, and samples with leaf particle size between 1.7 and 2 mm. All the BRDF values were measured using NASA Goddard Space Flight Center's (GSFC) Diffuser Calibration Laboratory (DCL) scatterometer [cf. Fig. 2(a) and (b)]. The typical measurement uncertainty was 1% $(k = 1)$ or better, where k is the coverage factor. The results presented are traceable to the National Institute of Standards and Technology's Spectral Trifunction Automated Reference Reflectometer.

The DCL has participated in several round-robin measurement campaigns with domestic and foreign calibration institutions in support of Earth and space satellite validation programs [3]. The facility has characterized many types of diffusely reflecting samples including Spectralon [4], aluminum diffusers, barium sulfate, radiometric tarps [5], and Martian regolith simulant [6].

The laboratory results were compared to BRDF measurements with an airborne radiometer, Cloud Absorption Radiometer (CAR), which was developed at GSFC [cf. Fig. 2(c)]

Manuscript received March 3, 2008; revised September 5, 2008. First published June 23, 2009; current version published July 23, 2009. This work was supported by the National Aeronautics and Space Administration under Agreement NAS5-02041 issued through the Science Mission Directorate.

G. T. Georgiev is with the Science Systems and Applications, Inc., Lanham, MD 20706 USA (e-mail: georgi.t.georgiev@nasa.gov).

C. K. Gatebe is with the Goddard Earth Sciences and Technology Center, University of Maryland, Baltimore County, Baltimore, MD 21228 USA.

J. J. Butler is with Hydrospheric and Biospheric Sciences Laboratory, NASA Goddard Space Flight Center, Greenbelt, MD 20771 USA.

M. D. King is with the Laboratory for Atmospheric and Space Physics, University of Colorado, Boulder, CO 80309 USA.

Color versions of one or more of the figures in this paper are available online at http://ieeexplore.ieee.org.

Digital Object Identifier 10.1109/TGRS.2009.2021331

0196-2892/$25.00 © 2009 IEEE

Authorized licensed use limited to: NASA Goddard Space Flight. Downloaded on August 23, 2009 at 21:04 from IEEE Xplore. Restrictions apply.

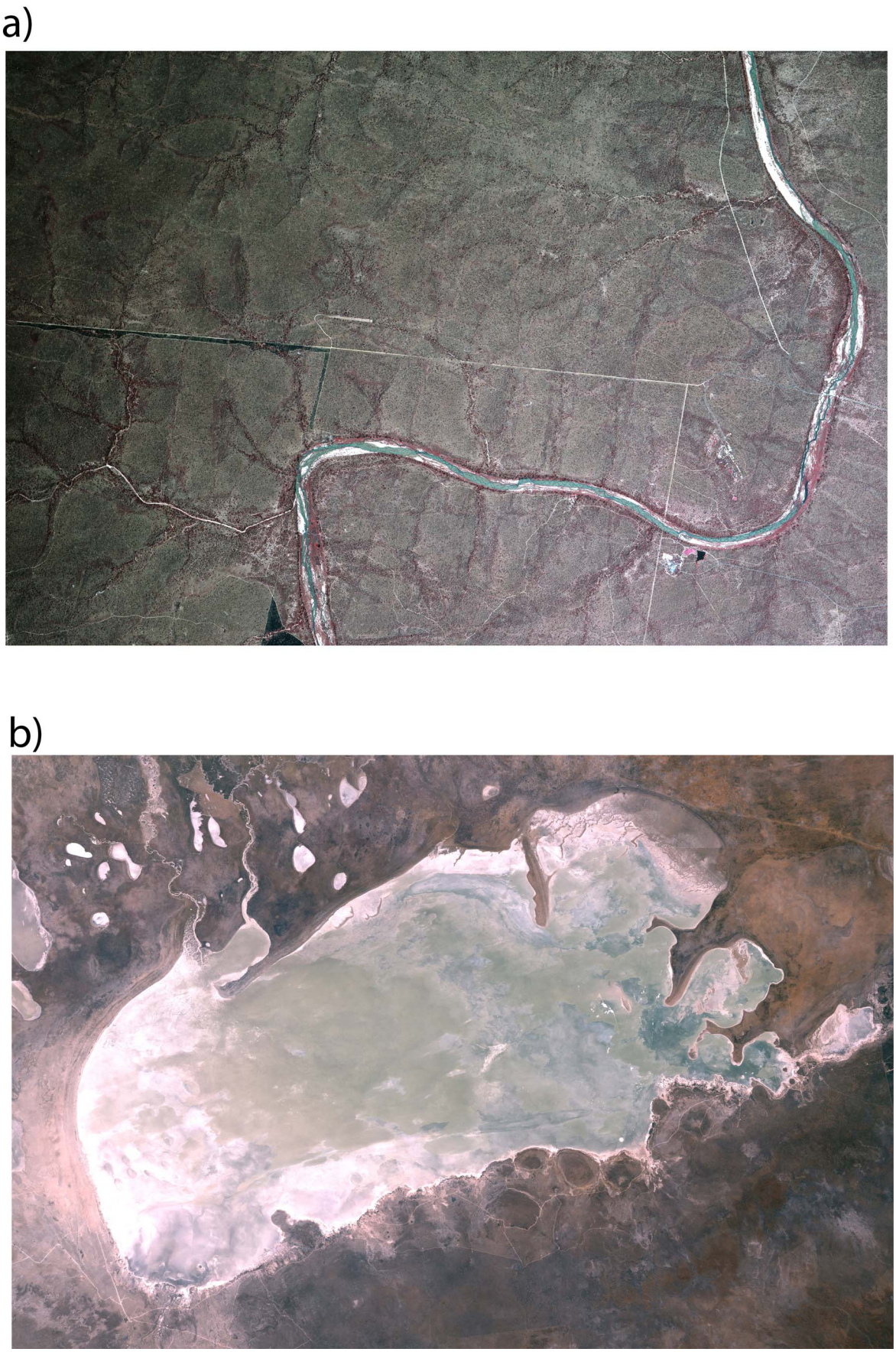

Fig. 1. (a) Skukuza. (b) Etosha Pan.

Authorized licensed use limited to: NASA Goddard Space Flight. Downloaded on August 23, 2009 at 21:04 from IEEE Xplore. Restrictions apply.

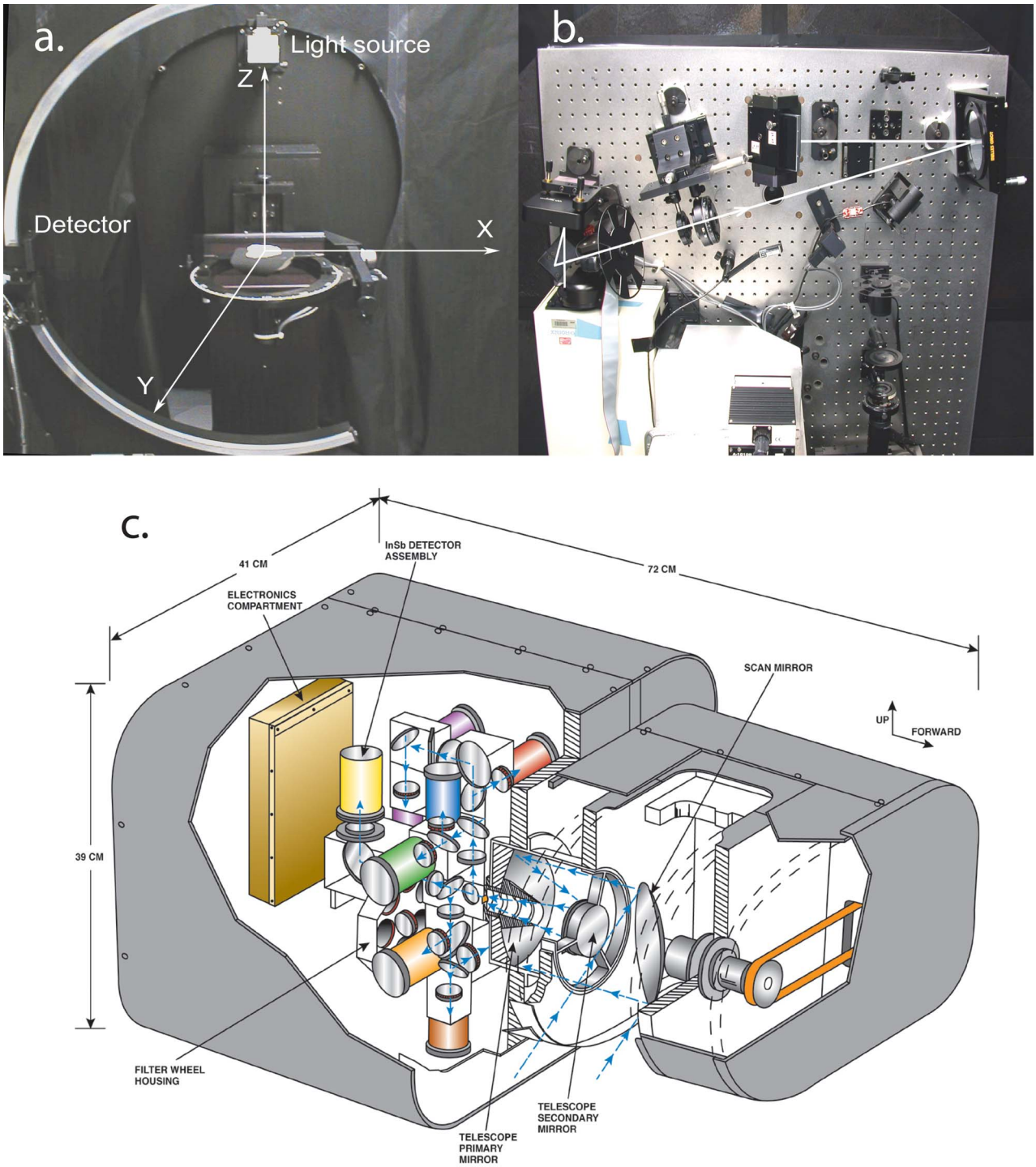

Fig. 2. (a) Scatterometer goniometer. (b) Scatterometer optical setup. (c) CAR instrument.

and described by King *et al.* [7] and Gatebe *et al.* [8]. The CAR is designed to scan from 5° before zenith to 5° past nadir, corresponding to a total scan range of 190°. Each scan of the instrument lies across the line that defines the aircraft track and extends up to 95° on either side of the aircraft horizon. The CAR field of view (FOV) is 17.5 mrad (1°), the scan rate is 1.67 Hz, the data system has nine channels at 16 bits, and it has 382 pixels in each scan line. CAR's 14 channels are located between 335 and 2344 nm. The CAR channels' exact wavelengths and bandpass widths are shown in Table I. These bands were selected to avoid atmospheric molecular-absorption bands in the near- and shortwave-infrared. In the normal mode of operation, data are sampled simultaneously and continuously on nine individual detectors. The first eight data channels between 335 and 1296 nm are always simultaneously and continuously sampled on eight individual detectors, while the ninth data channel is registered for signal selected from the six remaining channels on a filter wheel between 1530 and 2344 nm. The filter wheel can either cycle through all six wavelengths at a prescribed interval, usually changing filters every fifth scan line or lock

Authorized licensed use limited to: NASA Goddard Space Flight. Downloaded on August 23, 2009 at 21:04 from IEEE Xplore. Restrictions apply.

TABLE I
CAR SPECTRAL CHANNELS

Eight Continuously Sampled Channels		Six Filter Wheel Channels	
Spectral Channel	Wavelength (FWHM) (nm)	Spectral Channel	Wavelength (FWHM) (nm)
1	340 (9)	9	1556 (32)
2	381 (6)	10	1656 (45)
3	472 (21)	11	1737 (40)
4	682 (22)	12	2103 (44)
5	870 (22)	13	2205 (42)
6	1036 (22)	14	2302 (43)
7	1219 (22)		
8	1273 (23)		

onto any one of them, mostly 1656, 2103, or 2205 nm, and sample it continuously. Data are collected through the 190° aperture that allows observations of the earth–atmosphere scene around the starboard horizon from local zenith to nadir while the CAR scan mirror rotates 360° in a plane perpendicular to the direction of flight.

In this paper, the CAR data were obtained over Skukuza, South Africa, (25.0° S, 31.5° E) and Etosha Pan, Namibia (19.20° S, 15.93° E), which are core sites for validation of the Earth Observing System Terra and Aqua satellite instruments. These BRDF measurements are reported by Gatebe *et al.* [8]. A distinct backscattering peak in the principal plane characterizes the BRDF over Skukuza, whereas the BRDF over Etosha Pan is more enhanced in the backscattering plane and shows little directional variation.

II. METHODOLOGY

The definition and derivation of BRDF are credited to Nicodemus *et al.* [9], who presented a unified approach to the specification of reflectance in terms of both incident and reflected light-beam geometries for characterizing both diffuse and specular reflecting surfaces of optical materials. He defined the BRDF as a distribution function relating the irradiance incident from one given direction to the reflected radiance in another direction. Thus, the BRDF is presented in radiometric terms as the ratio of the radiance L_r reflected by a surface into the direction (θ_r, ϕ_r) to the incident irradiance E_i on a unit surface area from a specified direction (θ_i, ϕ_i) at a particular wavelength λ expressed mathematically as

$$\text{BRDF} = \frac{dL_r(\theta_i, \phi_i, \theta_r, \phi_r; E_i)}{dE_i\,(\theta_i, \phi_i)} \tag{1}$$

where the subscripts i and r denote incident and reflected light, respectively, θ is the zenith angle, and ϕ is the azimuthal angle. The BRDF units are sr^{-1}.

Nicodemus *et al.* further assumed that the incident beam has uniform cross section, the illumination on the sample is isotropic, and all scattering comes from the sample surface and none from the bulk. The bidirectional reflectance corresponds to directional–directional reflectance and ideally means that both incident and reflected light beams are collimated. Although perfect collimation and diffuseness are rarely achieved in practice, they can be used as a very useful approximation for reflectance measurements. In practice, we deal with real sample surfaces that reflect light anisotropically, and the optical beams used to measure the reflectance are not perfectly uniform. Hence, from a practical consideration, Stover [10] presented the BRDF in a convenient form for measurement applications. The BRDF is defined in radiometric terms as reflected surface radiance in a given direction divided by the incident surface irradiance from another or the same (i.e., retro) direction. The incident irradiance is the radiant flux incident on the surface. The reflected surface radiance is the light flux reflected through solid angle Ω per projected solid angle

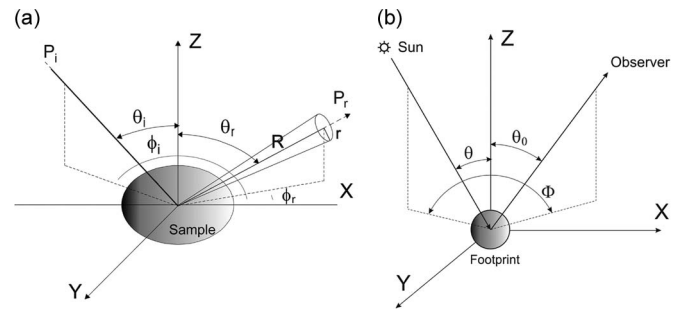

Fig. 3. Angular conventions. (a) BRDF. (b) BRF.

$$\text{BRDF} = \frac{\frac{P_r}{\Omega}}{P_i \cos\theta_r} \tag{2}$$

where P_r is the reflected radiant power and Ω is the solid angle determined by the area of detector aperture A and the radius from the sample to the detector R. The solid angle can be computed as $\Omega = A/R^2$. P_i is the incident radiant power, and θ_r is the reflected zenith angle. The $\cos\theta_r$ factor is a correction to account for the illuminated area, when viewed from the detector direction. BRDF has units of inverse steradians and can range from very small numbers (e.g., off-specular black samples) to very large values (e.g., highly reflective samples at specular reflectance). Following Stover's concept, the BRDF defining geometry is shown in Fig. 3(a), where the subscripts i and r refer to incident and reflected quantities, respectively. Note that the BRDF is often called cosine corrected, when the $\cos\theta_r$ factor is not included.

In the case of CAR measurements, the spectral BRDF (R_λ) is expressed following van de Hulst [11] formulation [see also Fig. 3(b)]:

$$R_\lambda(\theta, \theta_0, \Phi) = \frac{\pi I_\lambda(\theta, \theta_0, \Phi)}{\mu_0 F_\lambda} \tag{3}$$

where I_λ is the measured reflected intensity (radiance), F_λ is the solar flux density (irradiance) incident on the top of the atmosphere, θ and θ_0 are, respectively, the viewing and incident zenith angles, Φ is the azimuthal angle between the viewing and incident light directions, and $\mu_0 = \cos\theta_0$. The R_λ is equivalent to bidirectional reflectance factor (BRF) as defined

Authorized licensed use limited to: NASA Goddard Space Flight. Downloaded on August 23, 2009 at 21:04 from IEEE Xplore. Restrictions apply.

by Nicodemus *et al.*, which is dimensionless and numerically equivalent to BRDF times π.

The DCL scatterometer was used to measure the BRDF at different wavelengths and at different source and detector angular configurations. Although a more detailed design review on the scatterometer is published by Schiff *et al.* [12], we include in this paper some basic information. The scatterometer is located in a class 10 000 laminar-flow cleanroom. It is capable of measuring the BRDF and bidirectional transmission distribution function of a wide range of samples, including white- and gray-scale diffusers, black painted or anodized diffusers, polished or roughened metal surfaces, clean or contaminated mirrors, transmissive diffusers, liquids, and granular solids. The operational spectral range of the instrument is from 230 to 900 nm. The scatterometer can perform in the principal plane and out of the principal plane BRDF measurements. It consists of a vertical optical source table, a sample stage, a detector goniometer, and a computer system for positioning control, data collection, and analysis.

The optical table can be rotated around its horizontal axis located at the table center to change the incident angle θ_i relative to the sample normal [cf. Fig. 2(b)]. The optical source table contains two light sources—a 75 W xenon short-arc lamp coupled to a Chromex 250SM scanning monochromator and a replaceable coherent source in the operational spectral range. The scattered light from the sample is collected using an ultraviolet enhanced silicon photodiode detector with output fed to a computer controlled lock-in amplifier. The sample is mounted on a sample stage in the horizontal plane. The sample stage allows proper positioning of the sample with respect to the incident beam. It can be moved in X, Y, and Z linear directions using three motors. The sample stage provides sample rotation in the horizontal plane around the Z-axis, thereby enabling changes in the incident azimuthal angle ϕ_i. The standard scatterometer sample stage can accommodate samples as large as 45 cm^2 and up to 4.5 kg in weight. However, larger samples have been measured using custom designed sample adapters. As shown in Fig. 2(a), the detector assembly moves along the arc, providing the ability to make reflectance measurements as a function of the viewing zenith angle θ_r. The arc rotates 180° around the vertical Z-axis which determines the viewing azimuthal angle ϕ_r. The center of the illuminated spot on the surface of the sample has to be positioned at the cross point of the three perpendicular goniometer rotation axes, X, Y, Z, coinciding with the center of a sphere with radius equal to the distance between that point and the detector assembly's cover aperture.

The illuminated area on the sample underfills the FOV of the measurement detector. All measurements in this paper were made for polarizations of the incident beam parallel P and perpendicular S to the plane of incidence. The BRDF for each polarization was calculated by dividing the net signal from the reflected radiant flux by the incident flux and the projected solid angle from the calibration item to the limiting aperture of the detector. The BRDF values for both polarizations were then averaged to yield the BRDF for unpolarized incident radiant flux, and the values of the unpolarized scattering case are reported in this paper. The operation of the scatterometer is fully computerized. Customized software controls all motion, data acquisition, and data analysis.

III. Measurements

For the study described in this paper, we studied vegetative and soil samples from three different locations. The first location was Skukuza, South Africa; the second was Etosha Pan, Namibia; and the third was Maryland, U.S.

Skukuza [see Fig. 1(a)] is a well foliaged rest camp on the southern banks of Sabie River in southern Kruger National Park. The site exhibits typical savanna-ecosystem characteristics: more or less continuous vegetation cover with trees and shrubs in varying proportions. The differences in the composition, structure, and density of plant communities are attributable to the influence of the moisture in the area, as well as differences in the terrain: altitude and slope, as well as soil type and the prevalence of fires. The environment and vegetation of the flux measurement site near Skukuza is best described by Scholes *et al.* [13] and Pinheiro *et al.* [14]. The vegetation is dominated by savanna grass and knob thorn trees (*Acacia nigrescens*) with their flat relatively narrow crown and sparse canopy. They grow 5–18 m in height, are fire resistant, and are eaten by giraffes and other animals. The leadwood (*Combretum imberbe*) is also common. It normally grows up to 20 m, has a spreading, rather sparse, roundish to slightly umbrella shaped crown, and a single thick trunk.

The Skukuza samples shown in Fig. 4(a) were a < 2 mm diameter fraction of soil and dry leaf litter. The leaf litter is predominantly from acacia trees and savanna grass. The soil sample S1 is a coarse loamy sand soil with dominant grass roots from the top of the organic horizon, layer depth of 0–30 cm. The soil sample S2 is an exposed coarse loamy sand soil from the mineral horizon, layer depth 30–40 cm.

The Etosha Pan [see Fig. 1(b)] is 4590 km^2 in area and 120 km$\times$72 km in extent situated in northern Namibia. It is desertlike, white in color, and dry salt pan without any vegetation. During the rainy season, however, Etosha Pan becomes approximately a 10 cm deep lake and becomes a breeding ground for thousands of flamingos. Etosha Pan has unique reflective characteristics. Its reflectance spectra are high in the blue, around 440 nm. This explains the apparent white color of the pan as brighter objects in the blue part of the visible spectrum appear whiter to the human eye. The Etosha Pan mineralogy is dominated by four compounds: 1) feldspar and mica; 2) feldspar and sepiolite; 3) silicates; and 4) calcite and dolomite, which determine the pan's reflectance spectra. The Etosha Pan surroundings are dominated by mopane and acacia trees and grasslands. We studied four different fractions of Etosha Pan soil sample [see Fig. 4(b)]. The first Etosha sample, named in this paper as "the rock," is a solid piece of pan sediment, while the other three samples are regoliths with fractional sizes of 0.5 mm or less for Etosha Pan sample 1, hereinafter EP1, between 1 and 2 mm for EP2, and a submillimeter fraction for EP3.

In addition to Skukuza and Etosha Pan, samples from Maryland, U.S., consisting of whole, cut and crushed, and fresh and dried locust and poplar tree leaves were studied, as shown in Fig. 4(c) and (d). All samples were air dry at the time of this paper except the fresh locust and poplar samples. The cut and crushed samples were placed in a square $50 \times 50 \times 5$ mm black plastic holders with the sample surfaces well flattened. Care was taken for uniform particle distribution through the entire

Authorized licensed use limited to: NASA Goddard Space Flight. Downloaded on August 23, 2009 at 21:04 from IEEE Xplore. Restrictions apply.

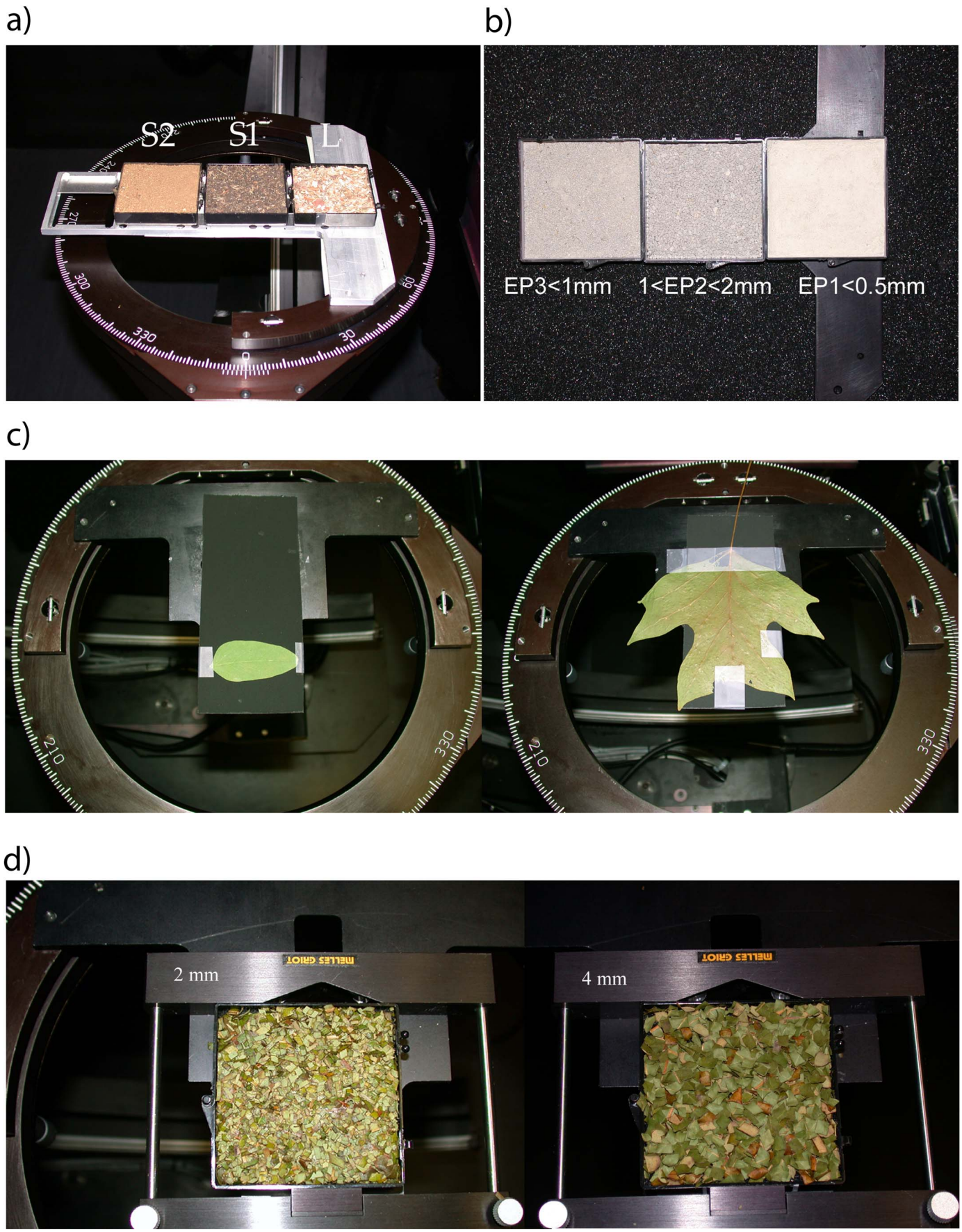

Fig. 4. (a) Skukuza leaf litter (L) and soil samples (S1) and (S2). (b) Etosha Pan samples EP1, EP2, and EP3. (c) Fresh locust and fresh poplar tree leaves. (d) 2- and 4-mm cut poplar tree leaves.

Authorized licensed use limited to: NASA Goddard Space Flight. Downloaded on August 23, 2009 at 21:04 from IEEE Xplore. Restrictions apply.

surface area. The holders were mounted horizontally on the sample stage and aligned with the scatterometer axes of rotation.

The laboratory study of Skukuza samples was done at the same wavelengths and incident and view angles as the CAR instrument airborne measurements over Skukuza. The incident angles for the Skukuza samples were 0° and 67°, the zenith view angles were from 0° to 80° with data acquired in steps of 5°, the azimuthal angles were 0° and 180° corresponding to the principal plane measurement geometry. The measurement wavelengths were 340, 470, and 870 nm, again based on CAR operating wavelengths. The top and bottom of the leaves were measured to account for structural differences such as smoothness and glossiness.

Similarly, Etosha Pan samples were studied at wavelengths and incident and view angles comparable to the airborne measurements over Etosha Pan. The Etosha Pan samples were characterized in the DCL at incident angles of 0°, 30°, and 60° and zenith view angles from 0° to 80° in steps of 5°. The DCL measurement wavelengths were 412, 555, 667, and 869 nm. However, only 667 and 869 nm correspond to the CAR's operational wavelengths.

The CAR instrument was flown aboard the University of Washington Convair CV-580 research aircraft during the Southern Africa Regional Science Initiative 2000 (SAFARI 2000) dry season campaign. The airborne CAR data from a vegetation rich surface were recorded over Skukuza during the dry season in August 2000 for view angles from $-80°$ to 80° and at a number of wavelengths. The BRDF of the savanna surface was acquired at 67° incident angle and viewing angles from $-80°$ to 80° in eight spectral bands from 0.34 to 1.27 μm. A hot spot or retroscatter signal was seen at about $-70°$. The airborne computed BRDF shows backscattering properties of the vegetation covered soil surface.

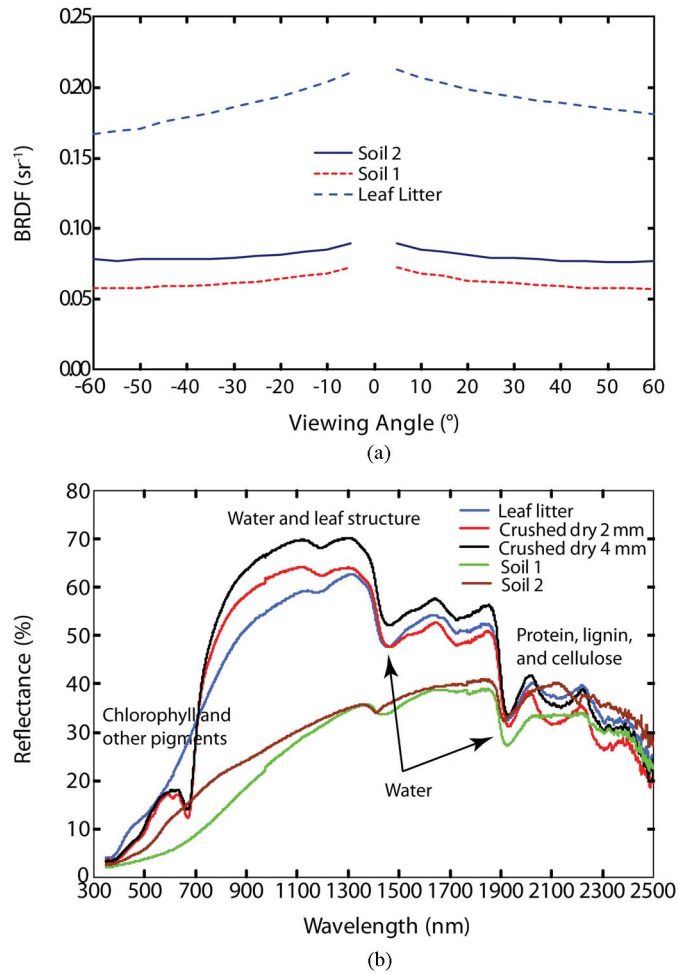

Fig. 5. (a) Laboratory-based BRDF of S1, S2, and L samples at normal incidence and 870 nm. (b) ASD reflectance spectra of S1, S2, and L samples and cut leaves at normal incidence and 60° viewing angle.

IV. Results and Discussion

A. Laboratory-Based BRDF of Savanna Samples, Skukuza

The laboratory-based BRDF at normal incidence for the two soils, S1 and S2, and a savanna leaf litter sample is shown in Fig. 5(a) at 870 nm. The BRDF at 340 and 470 nm is not shown in this paper as the view angle distribution is similar for those wavelengths. In addition to BRDF measurements, the samples' spectral reflectance was measured with an Analytical Spectral Device (ASD) spectroradiometer in-plane at 0° incident angle and 60° viewing angle from 350 to 2500 nm. The results are compared in Fig. 5(b), where the reflectance spectrum for fresh locust leaf taken at the same measurement geometry is also included. The leaves' complex biochemical composition made up of chlorophyll, pigments, proteins, starches, waxes, water, lignin, and cellulose is apparent in their reflectance spectra. The chlorophyll and pigments influence the spectra in the visible region. The water content and leaf structure contribute to the reflectance in the near-infrared, while the proteins, lignin, and cellulose contribute in the shortwave infrared [15].

The difference in BRDF of dry and fresh locust and poplar tree leaves at normal incidence is shown in Fig. 6(a) at 340 nm and in Fig. 6(b) at 470 nm. The overall reflectance of the locust dry leaves is higher at all wavelengths. Both fresh and dry poplar leaves have higher BRDF than the locust leaves at smaller scatter zenith angles (i.e., 0°–30°) and lower BRDF at larger scatter zenith angles (i.e., 30°–80°). The difference in BRDF between the two species illustrates the importance of accurate identification of the types of vegetation in airborne data recording. The percent difference of the BRDF varies between 20% and 60% depending on wavelength. The data at 340 and 470 nm are in the spectral region where mainly pigments dominate the leaf reflectance, whereas the BRDF at 870 nm is affected largely by the water content and leaf structure. For all leaves, there is also a difference in BRDF between the top and bottom sides of the leaves. On average, the bottom BRDF of the locust was always higher than the top BRDF: 34% higher at 340 nm, 48% at 470 nm, and 4% at 870 nm, due to the leaves' surface structure.

In order to address the vegetation canopy remote sensing scaling problem, we measured the BRDF of cut fresh leaves and crushed dry leaves. The reflectance of a scene as seen from an airborne (or spaceborne) sensor depends on the reflectance of its components and their composition. It was estimated that, for airborne BRDF measurements of land surfaces from a 600 m altitude, the average footprint of a 4–5 m in diameter of a typical savanna tree would correspond to a leaf particle size in the laboratory of ~4 mm, whereas the footprint of a typical savanna bush, 1.5–2 m in diameter would correspond to a leaf particle size of ~2 mm. The BRDFs of 2- and 4-mm-size leaves

Authorized licensed use limited to: NASA Goddard Space Flight. Downloaded on August 23, 2009 at 21:04 from IEEE Xplore. Restrictions apply.

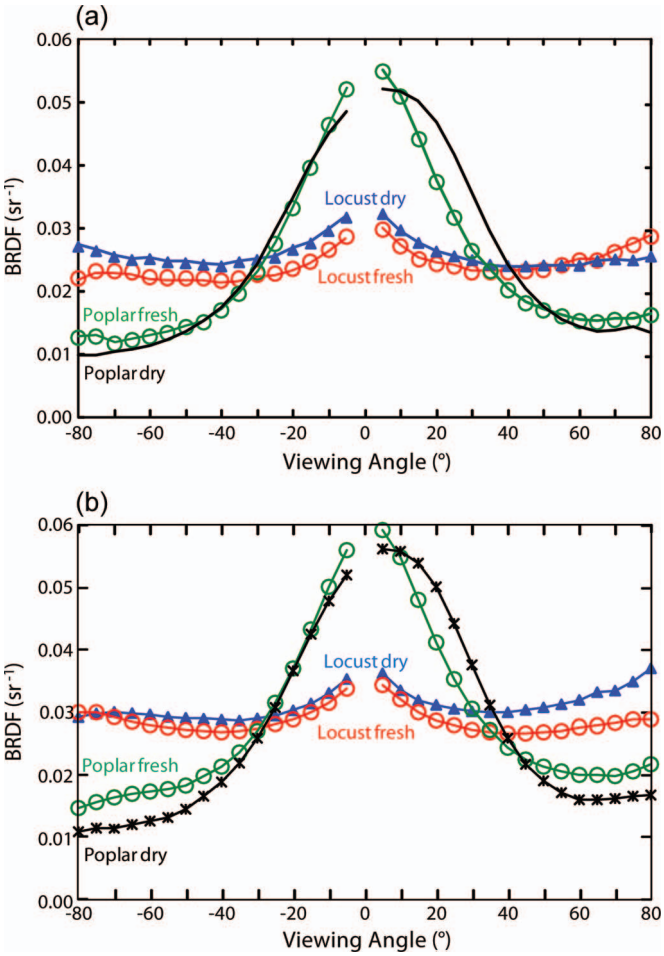

Fig. 6. Laboratory-based BRDF of locust and poplar tree dry and fresh leaves at normal incidence. (a) 340 nm. (b) 470 nm.

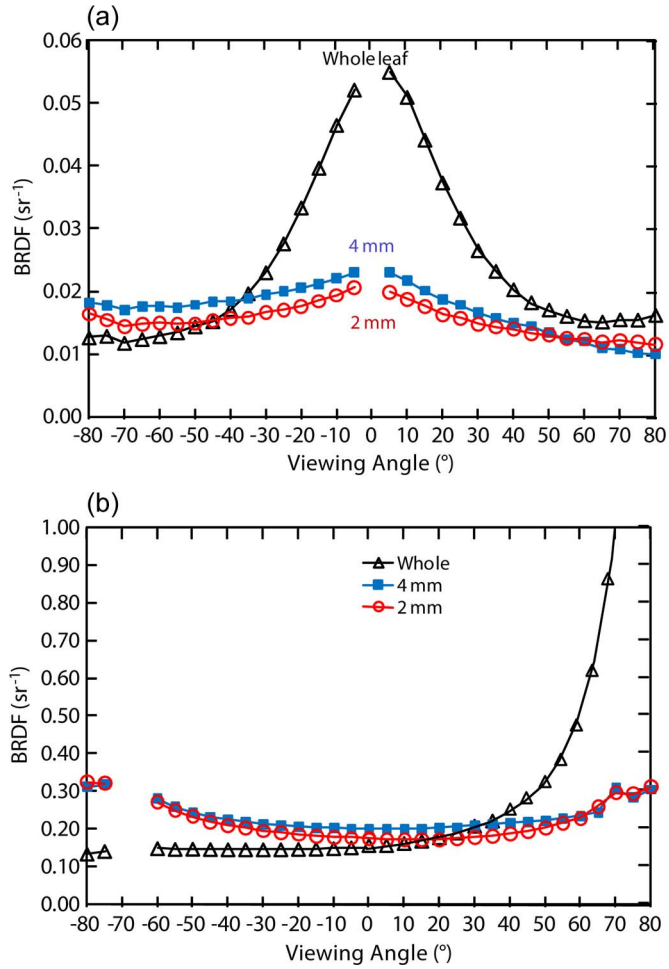

Fig. 7. Laboratory-based BRDF of whole, 4-, and 2-mm cut poplar leaves at (a) normal incidence and 340 nm and (b) 67° incidence and 870 nm.

particles (cut fresh, crushed dry) and whole fresh and dry leaves were compared.

The differences in the case of poplar leaves at 340 nm are shown in Fig. 7(a) at normal incidence. Significant differences occur between the measured BRDFs of whole and crushed leaves at small viewing angles from 5° to 45°. The percent differences between the BRDF of whole leaves and crushed leaves having a 4 mm particles size are up to 55% at 5° viewing angle and up to 59% for the 2 mm sample. The differences at scatter angles from 45° to 80° are on the order of 27% at 80° viewing angle for whole leaves versus 4 mm crushed leaves and 18% for whole leaves versus 2 mm crushed leaves. The possible explanation for this is that the scatter from the whole leaf has a strong specular component, leading to higher reflectance at small scatter angles. The scatter from the crushed leaves is more diffused, resulting in much lower BRDF at small angles. The second reason for the different BRDF is the shadowing effect that takes place when the surface of a sample is not flat but consists of small particles. In the crushed-leaf BRDF sample, the scattering between the individual leaf particles is a significant contributor to the reflected distribution of scattered light. The BRDF of the 4 mm sample is higher than the BRDF of the 2 mm sample. The smaller particles exhibit less extensive shadowing when illuminated; however, the light-obscuration effect when viewing by the detector is stronger. The difference in the BRDF of 2 and 4 mm samples is relatively small and is not a strong function of increasing scatter angle. We also observed the same BRDF relation at other wavelengths.

Whole, 2, and 4 mm poplar leaves were measured at an incident angle of 67°, as shown in Fig. 7(b), which shows data acquired at 870 nm. For non-normal illumination geometries, the leaves exhibit strong forward scattering at all wavelengths for both fresh and dry samples. The backscattering is stronger for the dry samples. The BRDF of fresh and dry poplar leaves at 67° incident angle were compared at 340, 470, and 870 nm. The BRDF is lower at shorter wavelengths; however, the scattered-light view-angle distribution pattern is largely independent of wavelength. The glossy surface of a whole leaf has a well-pronounced specular component, whereas the crushed samples show predominantly diffuse scattering. The shadowing effect of the sample particles is also evident at 67° incident angle.

The soil and leaf litter samples' BRDF are shown in Fig. 8 at 340 and 870 nm. The BRDF distribution depends strongly on the nature of the sample (i.e., soil versus leaf) and the viewing angle. The soil samples, S1 and S2, exhibit enhanced optical backscattering. The leaf litter sample L, however, behaves differently. The L sample exhibits equal forward scattering at 340 nm, as shown in Fig. 8(a), and enhanced backscattering at 470 and 870 nm [Fig. 8(b)] (470 nm data not shown). The enhanced backscattering in the L sample is seen to increase

Authorized licensed use limited to: NASA Goddard Space Flight. Downloaded on August 23, 2009 at 21:04 from IEEE Xplore. Restrictions apply.

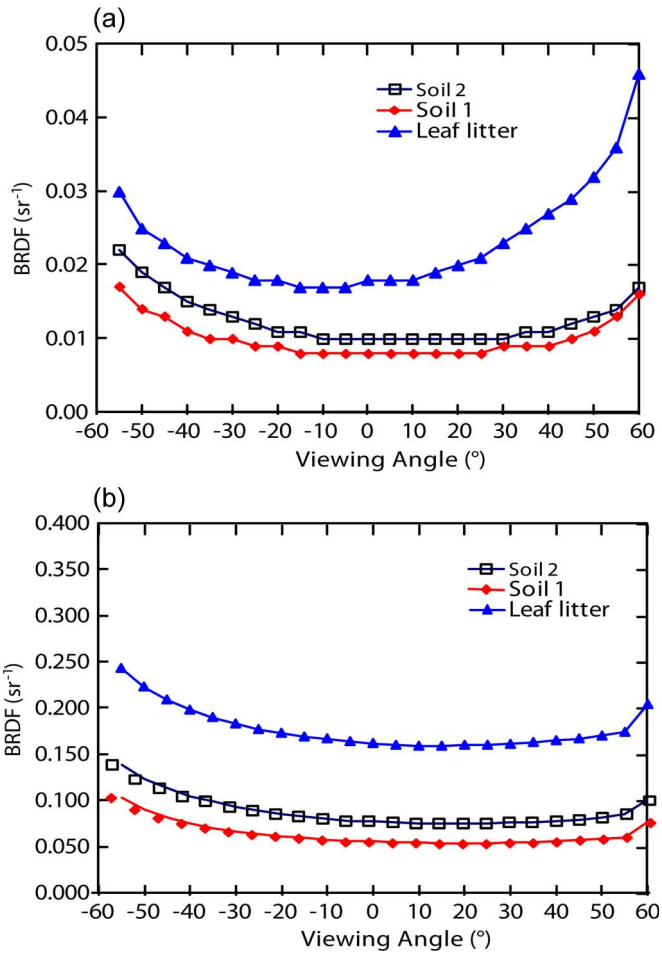

Fig. 8. Laboratory-based BRDF of soil and leaf litter at 60° and (a) 340 and (b) 870 nm.

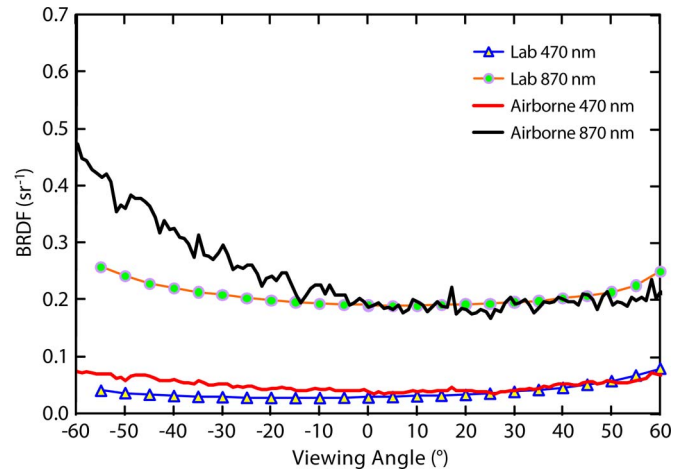

Fig. 9. Simulated-scene BRDF from the fractional laboratory-based BRDF measurements and CAR airborne data at 470 and 870 nm.

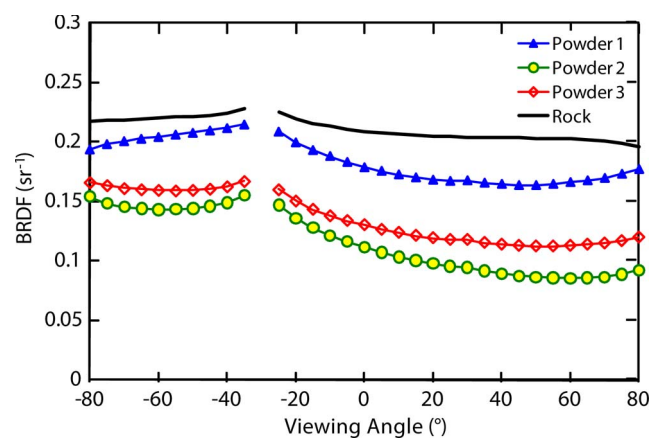

Fig. 10. Laboratory-based BRDF of Etosha Pan samples at 30° incident angle and 667 nm.

with increasing wavelength. Although the BRDF at $\theta_i = \theta_r$ could not be measured due to the relative geometries of the scatterometer source optics and detector, the BRDF for all samples show evidence of a significant opposition effect, which is represented by increased light being retroscattered back in the direction of the incident beam.

In order to compare the laboratory-based BRDF with the airborne measurements, we calculated a composite laboratory-based BRDF from the following laboratory-measured BRDF of four different samples: fresh and dry locust leaves, crushed leaf litter, and soil samples. The ratio of each sample used to produce the composite laboratory-based BRDF was determined by the distribution of the four components as seen by the CAR instrument during its airborne missions. From a careful examination of photographs taken over Skukuza during SAFARI 2000, we estimated that the vegetation cover was 90% (80% fresh, 10% dry), 5% exposed leaf litter, and 5% exposed soil. The vegetation includes tree canopies as well as savanna grass. The simulated scene BRDF from the fractional laboratory-based BRDF measurements and CAR airborne data are shown in Fig. 9.

The same general shape of the BRDF of the laboratory-measured samples and airborne measurements can be seen in the data shown in Fig. 9. The BRDF matches very well from 0° to 60° viewing angle at 470 nm and from −15° to 60° viewing angle at 870 nm. However, there is a significant deviation between the laboratory and airborne data at increasingly negative scatter angles, corresponding to backscatter directions. The identification of the sources of differences in laboratory and airborne BRDF measurements through quantification of their effects on measured BRDF is an ongoing goal of this paper. For example, we have not accounted for 3-D effects such as tree heights, which would have significant effect on BRDF at a lower sun elevation, particularly in the principal plane at the airborne measurements.

B. Laboratory-Based BRDF of Salt Pans, Etosha Pan

The laboratory-based BRDF at 30° incidence for the four Etosha Pan samples is shown in Fig. 10 at 667 nm. The rock sample's BRDF is higher as the particulate incident light-shadowing and scatter light obscuration effects are the smallest. The finest structure sample, EP1, has distinctively higher BRDF than the two other larger fractions, samples EP2 and EP3. It is worth noting that the shape of the BRDF curve for the rock sample is different than the shape of the regolith samples. It is also very important that all samples have apparent backscattering properties. Although the BRDF at $\theta_i = \theta_r$ could not be measured due to the relative geometries of the scatterometer

Authorized licensed use limited to: NASA Goddard Space Flight. Downloaded on August 23, 2009 at 21:04 from IEEE Xplore. Restrictions apply.

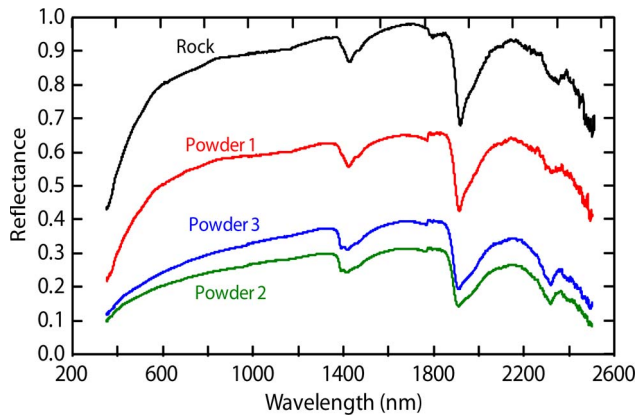

Fig. 11. ASD reflectance of Etosha Pan samples at 30° incident angle and 30° scatter zenith angle.

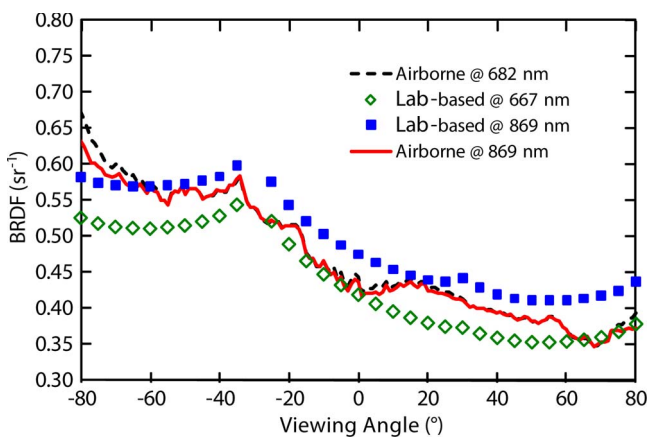

Fig. 12. Etosha Pan simulated-scene BRDF from the fractional laboratory-based BRDF and CAR airborne data.

source optics and detector, the BRDF for all samples shows evidence of a significant opposition effect represented by increased light being retroscattered back in the direction of the incident beam. Sample EP2, with particle sizes between 1 and 2 mm, has the lowest BRDF. In addition to BRDF measurements, the samples' spectral reflectance was measured with an ASD spectroradiometer in-plane at 30° incident angle and 30° angle from 350 to 2500 nm (see Fig. 11). The ASD reflectance spectra present a full reflectance picture for the VIS-NIR spectral range providing additional information on the Etosha Pan sample's reflectance properties.

In order to correctly compare the laboratory-based BRDF with the airborne measurements, we calculated the composite laboratory based BRDF from the laboratory measured BRDF of the three different Etosha Pan samples. The ratio of each sample in the calculated laboratory-based BRDF was determined by the distribution of the three components as seen by the CAR instrument during the airborne measurements. From a careful examination of photographs of Etosha Pan, the components were determined to be 25% EP1, 50% EP2, and 25% EP3. The simulated fractional laboratory-based data are compared to the CAR airborne data in Fig. 12.

The same general shape of the laboratory-measured samples and airborne measurements is shown in Fig. 12. The data match well within the uncertainty for both wavelengths all over the viewing angular range with the exception of $-80°$, where the CAR measured data are slightly higher. However, the airborne data at those two wavelengths are very close. The laboratory-based data at 667 and 869 nm show a larger difference than the CAR data at those wavelengths.

V. Conclusion

This paper is intended to describe more completely the BRDF of savanna vegetation and soil samples from Skukuza and soil samples from Etosha Pan measured in a laboratory environment. In addition, the laboratory results are compared to *in situ* measurements of these areas by the CAR instrument. In the laboratory measurements, the BRDF depends on the incident and viewing angles, on the nature of the sample (i.e., crushed versus whole leaf), on the sample status (fresh versus dry), on the sample biochemical composition for Skukuza samples, and on the particle size fraction for Etosha Pan samples. The analysis shows strong spectral dependence of the BRDF data on the leaf biochemical composition. The BRDF of the locust whole leaf bottom was always higher than the BRDF of the top of the same leaf, due to the surface physical structure. The difference in BRDF between the two plant species, locust and tulip poplar, can be as high as 100%, illustrating the importance of knowing the vegetation type for airborne measurements. The difference between the BRDF of whole leaves, 4, and 2 mm crushed leaves can be as high as 55% at 5° scatter zenith angle due to a strong specular component for the whole leaf sample and the presence of incident light shadowing and scattered light obscuration for the crushed leaves samples. The laboratory-based BRDF of Etosha Pan samples depend on sample fraction. It is highest for the rock sample and lowest for the larger size particles regolith sample.

Laboratory-based and CAR airborne data sets were compared at 470 and 870 nm for Skukuza. They matched very well from 0° to 60° viewing angle at 470 nm and from $-15°$ to 60° viewing angle at 870 nm. However, there is a discrepancy between the laboratory and airborne data at negative viewing angles, particularly at higher angles. We examined the difference between the optical scattering properties of fresh and dried vegetation in an effort to identify possible source for this difference. The degree of senescence of vegetation is one potential source for this difference. Laboratory-based and CAR airborne data sets from Etosha Pan were compared at 682 and 870 nm for the airborne data and 677 and 869 nm for the laboratory data, respectively. The BRDF curves have the same general shape, and the data matches well into the uncertainty for both wavelengths over all viewing angular range. However, the airborne data show smaller BRDF differences between the two wavelengths than the laboratory-based data. Although the effects of atmospheric absorption and scattering were removed from CAR measurements [8], the process is uncertain considering the assumptions made such as aerosol particle shape, which is assumed spherical, and vertical distribution, which is assumed to be homogenously mixed. Note that atmospheric correction is not so important in laboratory measurements. The wavelength difference between airborne and laboratory data is also a source of difference in the BRDF. We believe that the laboratory results are of great use to the remote sensing community in their modeling and correction efforts of airborne data.

Authorized licensed use limited to: NASA Goddard Space Flight. Downloaded on August 23, 2009 at 21:04 from IEEE Xplore. Restrictions apply.

REFERENCES

[1] J. J. Butler, B. C. Johnson, and R. A. Barnes, "The calibration and characterization of Earth remote sensing and environmental monitoring instruments," in *Optical Radiometry*, A. C. Parr, R. U. Datla, and J. L. Gardner, Eds. New York: Academic, 2005, pp. 453–534.

[2] G. P. Asner, C. A. Wessman, D. S. Schimel, and S. Archer, "Variability in leaf and litter optical properties: Implications for BRDF model inversions using AVHRR, MODIS, and MISR," *Remote Sens. Environ.*, vol. 63, no. 3, pp. 243–257, Mar. 1998.

[3] E. A. Early, P. Y. Barnes, B. C. Johnson, J. J. Butler, C. J. Bruegge, S. F. Biggar, P. S. Spyak, and M. M. Pavlov, "Bidirectional reflectance round-robin in support of the Earth observing system program," *J. Atmos. Ocean. Technol.*, vol. 17, no. 8, pp. 1077–1091, Aug. 2000.

[4] G. T. Georgiev and J. J. Butler, "Long-term calibration monitoring of Spectralon diffusers BRDF in the air-ultraviolet," *Appl. Opt.*, vol. 46, no. 32, pp. 7892–7899, Nov. 2007.

[5] G. T. Georgiev and J. J. Butler, "Laboratory-based bidirectional distribution functions of radiometric tarps," *Appl. Opt.*, vol. 47, no. 18, pp. 3313–3323, Jun. 2008.

[6] G. T. Georgiev and J. J. Butler, "Bidirectional reflectance distribution function and directional–hemispherical reflectance of a Martian regolith simulant," *Opt. Eng.*, vol. 44, no. 3, p. 036 202, Mar. 2005.

[7] M. D. King, M. G. Strange, P. Leone, and L. R. Blaine, "Multiwavelength scanning radiometer for airborne measurements of scattered radiation within clouds," *J. Atmos. Ocean. Technol.*, vol. 3, no. 3, pp. 513–522, Sep. 1986.

[8] C. K. Gatebe, M. D. King, S. Platnick, G. T. Arnold, E. F. Vermote, and B. Schmid, "Airborne spectral measurements of surface–atmosphere anisotropy for several surfaces and ecosystems over southern Africa," *J. Geophys. Res.*, vol. 108, no. D13, p. 8489, Mar. 2003. DOI: 10.1029/2002JD002397.

[9] F. E. Nicodemus, J. C. Richmond, J. J. Hsia, I. W. Ginsburg, and T. Limperis, "Geometrical considerations and nomenclature for reflectance," Nat. Bureau Standards, Washington, DC, NBS Monograph 160, 1977.

[10] J. C. Stover, *Optical Scattering: Measurement and Analysis*. Bellingham, WA: SPIE, 1995.

[11] H. C. van de Hulst, *Multiple Light Scattering, Tables, Formulas, and Applications*, vol. 1. San Diego, CA: Academic, 1980.

[12] T. F. Schiff, M. W. Knighton, D. J. Wilson, F. M. Cady, J. C. Stover, and J. J. Butler, "Design review of a high-accuracy UV to near infrared scatterometer," *Proc. SPIE*, vol. 1995, pp. 121–130, Dec. 1993.

[13] R. J. Scholes, N. Gureja, M. Giannecchinni, D. Dovie, B. Wilson, N. Davidson, K. Piggott, C. McLoughlin, K. van der Velde, A. Freeman, S. Bradley, R. Smart, and S. Ndala, "The environment and vegetation of the flux measurement site near Skukuza, Kruger National Park," *Koedoe*, vol. 44, no. 1, pp. 73–83, 2001.

[14] A. C. T. Pinheiro, J. L. Privette, and P. Guellevic, "Modeling the observed angular anisotropy of land surface temperature in a savanna," *IEEE Trans. Geosci. Remote Sens.*, vol. 44, no. 4, pp. 1036–1047, Apr. 2006.

[15] R. F. Kokaly and R. N. Clark, "Spectroscopic determination of leaf biochemistry using band-depth analysis of absorption features and stepwise multiple regression," *Remote Sens. Environ.*, vol. 67, no. 3, pp. 267–287, Mar. 1999.

Georgi T. Georgiev (M'07) received the Diploma degree in engineering from Budapest Technical University, Budapest, Hungary, and the Ph.D. degree in physics from the Bulgarian Academy of Sciences, Sofia, Bulgaria, in 1998.

He was with the University of Maryland, College Park, where he worked on projects of the NASA Goddard Space Flight Center, Greenbelt, MD, on acoustooptic imaging spectroscopy for space applications. He was a Research Scientist with the Central Laboratory of Mineralogy and Crystallography, Bulgarian Academy of Sciences. He is currently with the Science Systems and Applications, Inc., Lanham, MD, and also with the Calibration Facility, NASA Goddard Space Flight Center. His research interests are in the fields of optical scattering and diffraction and acoustooptics. He is involved in instrument development and measurements of bidirectional scattering distribution functions in the ultraviolet through shortwave-infrared wavelength regions on a variety of optical and nonoptical materials. His publications reflect research interests in optical scattering and acoustooptic devices.

Dr. Georgiev is a member of SPIE and the Optical Society of America.

Charles K. Gatebe received the B.Sc. degree in meteorology, mathematics, and physics and the M.Sc. degree in meteorology from the University of Nairobi, Nairobi, Kenya, in 1990 and 1994, respectively, and the Ph.D. degree in atmospheric sciences from the University of the Witwatersrand, Johannesburg, South Africa, in 1999.

From 1995 to 1998, he was with the Institute of Nuclear Science, University of Nairobi, where he taught courses on air pollution using nuclear-related techniques. In 1999, he was a Resident Research Associate of the Universities Space Research Association with the NASA Goddard Space Flight Center (GSFC). He is currently an Associate Research Scientist with the Goddard Earth Sciences and Technology Center, University of Maryland, Baltimore County, Baltimore, MD, where he is based at GSFC. His interests include airborne measurements of bidirectional reflectance distribution function over different types of surfaces to elaborate important surface and atmosphere radiative-transfer functions and improve remote-sensing retrievals of aerosols and clouds.

Dr. Gatebe was the recipient of the World Meteorological Organization Young Scientist Award in 2000 and was honored in 2008 by NASA GSFC's Climate and Radiation Branch for his outstanding scientific leadership in conducting airborne measurements.

James J. Butler received the B.S. degree in physical chemistry from the University of Notre Dame, Notre Dame, IN, in 1977 and the Ph.D. degree in physical chemistry from the University of North Carolina, Chapel Hill, in 1982.

He is currently an Optical Physicist with the Hydrospheric and Biospheric Sciences Laboratory, NASA Goddard Space Flight Center (GSFC), Greenbelt, MD, where he has been a Research Scientist since 1984. Since January 1995 and January 2003, he has been performing the duties of EOS Calibration Scientist and NASA's representative to the NPOESS Joint Agency Requirements Group, respectively. Since June 2004, he has also been serving as NASA's Deputy Project Scientist for instruments and calibration within the NPOESS Preparatory Project. He also manages the NASA/GSFC Diffuser Calibration Facility. His previous research experience at NASA includes ground-based and balloonborne lidar for the detection of stratospheric molecular and radical species and laser-induced fluorescence of molecules and radicals.

Michael D. King (M'01–SM'03) received the B.A. degree in physics from Colorado College, Colorado Springs, in 1971 and the M.S. and Ph.D. degrees in atmospheric sciences from the University of Arizona, Tucson, in 1973 and 1977, respectively.

From 1992 to 2008, he was a Senior Research Scientist with the NASA Goddard Space Flight Center, Greenbelt, MD, where he served as Senior Project Scientist of NASA's Earth Observing System. Since April 2008, he has been with the Laboratory for Atmospheric and Space Physics, University of Colorado, Boulder. As a member of the MODIS Science Team, he is responsible for algorithms being run routinely to process MODIS data on the Terra and Aqua satellites to derive cloud optical and microphysical properties of liquid water and ice clouds. His research experience includes conceiving, developing, and operating multispectral scanning radiometers from a number of aircraft platforms in field experiments ranging from arctic stratus clouds to smoke from the Kuwait oil fires in the Persian Gulf and biomass burning in Brazil and southern Africa.

Dr. King is a Fellow of the American Geophysical Union and the American Meteorological Society and a member of the U.S. National Academy of Engineering. He was the recipient of the IEEE Prize Paper Award in 1993.

Authorized licensed use limited to: NASA Goddard Space Flight. Downloaded on August 23, 2009 at 21:04 from IEEE Xplore. Restrictions apply.